


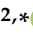


Article

Engineering SERS Properties of Silicon Nanotrees at the Nanoscale

Hrvoje Gebavi ^{1,2}, Petra Pál ³ , István Csarnovics ³ , Vlatko Gašparić ^{1,2}  and Mile Ivanda ^{1,2,*} 

¹ Laboratory for Molecular Physics and Synthesis of New Materials, Division of Materials Physics, Ruđer Bošković Institute, Bijenička cesta 54, 10 000 Zagreb, Croatia

² Research Unit New Functional Materials, Center of Excellence for Advanced Materials and Sensing Devices, Bijenička cesta 54, 10 000 Zagreb, Croatia

³ Department of Experimental Physics, Institute of Physics, Faculty of Science and Technology, University of Debrecen, Bem tér 18/a, 4026 Debrecen, Hungary

* Correspondence: ivanda@irb.hr

Abstract: Large specific surface area nanostructures are desirable in a wide range of sensing applications due to their longer light-trapping path and increased absorption. Engineering of the specific nanotree structure which possesses a high branch density turned out to be challenging from the experimental point of view, and certainly not adequately explored. This paper shows how to design substrates with a silicon nanotree structure for surface-enhanced Raman spectroscopy (SERS) applications. Silicon nanotrees were synthesized by a Ag–Au nanocluster-catalyzed low-pressure chemical vapor deposition method (LPCVD). By the presented approaches, it is possible to manipulate branches' number, length and thickness. The synthesized nanostructures are flexible after immersion in water which improves SERS performance. The amount of sputtered metal played a key role in preserving the flexibility of the nanotree structure. The obtained substrates with highly fractal nanostructure were tested on 4-mercaptophenylboronic acid (MPBA) to match the optimal SERS parameters. The silicon nanotrees fabrication, and particularly obtained SERS substrates plated with Ag and Au nanoparticles, demonstrated good features and a promising approach for further sensor development.

Keywords: surface-enhanced Raman spectroscopy (SERS); Si nanotrees; vapor–liquid–solid (VLS) method; low-pressure chemical vapor deposition (LPCVD); Ag and Au nanoparticles; 4-mercaptophenylboronic acid detection; SERS substrates optimization



Citation: Gebavi, H.; Pál, P.; Csarnovics, I.; Gašparić, V.; Ivanda, M. Engineering SERS Properties of Silicon Nanotrees at the Nanoscale.

Chemosensors **2022**, *10*, 534.

<https://doi.org/10.3390/chemosensors10120534>

Academic Editors: Natércia Martins and Sara Fateixa

Received: 21 October 2022

Accepted: 9 December 2022

Published: 15 December 2022

Publisher's Note: MDPI stays neutral with regard to jurisdictional claims in published maps and institutional affiliations.



Copyright: © 2022 by the authors. Licensee MDPI, Basel, Switzerland. This article is an open access article distributed under the terms and conditions of the Creative Commons Attribution (CC BY) license (<https://creativecommons.org/licenses/by/4.0/>).

1. Introduction

The nanotree (NTr), also known as branched nanowire, consist of a nanowire-trunk as a backbone and radial, smaller-dimension branches [1]. As a result of large specific surface area and direct electron transport pathways, NTrs have found numerous applications in fields such as energy materials (batteries, photovoltaics, photocatalysis, photoelectrochemical water splitting, supercapacitors, etc.) [2–5], nanoelectronics devices [6], gas sensors [7], and bioelectronics [8]. NTrs can be categorized depending on: (a) the level of complexity (single [9] or hyper-branched [10–12]) and (b) the composition material (homostructured [7,10,13] or heterostructured [14–16]).

The most common method for silicon nanotrees (SiNTr) growth is the vapor–liquid–solid (VLS) method [17–21]. Generally, the NTr growth includes the main trunk growth and, subsequently, the branches. The branches can be grown within the same experiment or after the additional metal catalyst plating, followed by an additional VLS-deposition experiment [3]. If the trunks and branches are grown within one experiment, the catalyst diffusion is induced by an increase or decrease of either temperature [22] or partial pressure [6]. To obtain NTrs, a key point is to control thermodynamics in the following synthesis stages: (a) trunks growth, (b) catalyst diffusion and (c) branches' growth. (a) Trunk

thickness and height are mainly influenced by temperature, gas pressure and deposition time. Their number per unit area can be increased by additional Ag coating before the traditional Au seed layer [21]. (b) In ref. [23] authors introduced an annealing step before branch growth. By holding the same temperature as for the trunks' growth, the active SiCl_4 gas was removed while the pressure of the carrier gas H_2 was kept constant. After that, the branches' growth was activated by releasing the SiCl_4 under the same pressure as the trunks' growth. The catalyst diffusion depends on the activation method and annealing time, which consequently determines the branches' position and number. (c) Branches can be obtained by manipulating the gas pressure during the VLS process while keeping the temperature constant [24]. After the trunk growth, the gas flow was gradually reduced, and after a short period, increased to induce the branches' growth. The critical, i.e., minimum possible branch radius is dependent on partial gas pressure since it is correlated with the supersaturation within the Au/Si droplet. Furthermore, the atomic percentage of silicon in the droplet of ~23–24% for branches with 5–25 nm in radius synthesized at $T = 500\text{ }^\circ\text{C}$ is indicated [6]. The branch density can be controlled by the catalyst–nanodroplets concentration [25] in the two-step approach, while the length and thickness by deposition duration. However, the second metal catalyst plating has its disadvantages such as environmental oxidation, and therefore oxygen removal by HF. This includes substrates pouring into a liquid, and consequently, a subtle trunk morphology change.

Apart from that, transitions between these three synthesis stages can be delicate as well. The duration of each stage determines whether the branches will grow as well as their morphological characteristics. For example, very short trunk growth at a low temperature (~500 °C) leads to thin wires growth which makes the branches' growth difficult. Furthermore, a short catalyst diffusion time does not allow an adequate diffusion along the trunk length, i.e., it determines the branches' number, position and mutual separation. A decrease in the growth temperature with enhanced Silane flux is reported as the best way to produce NTrs [26]. On the contrary, it is reported that instead of a decrease, a sharp increase in temperature and gas flow velocity, may cause a breakdown of the liquid droplet on the nanowire tip, accompanied by further branching [27].

Another important parameter for SiNTr growth is oxygen content [23]. They observed branches' growth in the case of annealing in $\text{Ar} + \text{H}_2$ gas flow whereas annealing in only Ar flow was not successful. Utilization of H_2 and SiCl_4 indicated that an oxygen-free atmosphere is a prerequisite for NTr growth. On the other hand, they claim that there is no need to synthesize NTr in an ultra-pure oxygen atmosphere since a small amount of residual surface or atmosphere oxygen (order of ppm) inhibits the eutectic alloy migration.

This paper shows a SiNTr synthesis process targeting sensor development. The first goal is to describe how to synthesize SiNTrs without additional metal plating, i.e., single-step synthesis. The two-step synthesis includes a catalyst and surface oxygen removal [3] before the second metal plating. Those processes include immersion in solution (I_2 and KI), HF acid and purified water. However, immersion in liquids and drying would induce SiNW bundling via capillary forces and one would lose the 'tweezers effect', one of the crucial factors for high SERS enhancement [20]. The second target is to synthesize a high surface area nanostructure. This goal is characteristic of numerous sensors since the high surface area leads to an increased number of available sites for a specific reaction (in the field of SERS called 'hot spots'), thereby increasing the sensor's efficiency. Although SiNTr nanostructure can be applied to a wide range of sensors, this paper is more oriented toward the development of substrates for SERS. Apart from targeting a high surface area, a particularity of SERS sensors is that they can be flexible in nanostructure, which is our third goal. The flexible nanostructure additionally benefits SERS efficiency through the 'tweezers' mechanism as described in [20,28].

Although the literature has reported the synthesis of SiNTrs [23,24,26,29,30], there is a lack in some of the following points: a high SiNTr number per unit area, a high-density branch growth along the trunks' facets, reduction of trunk regrowth, flexible nanostructure

and SERS enhancement demonstration. This work overcomes the present issues and shows a novel SiNTr synthesis approach.

2. Experimental

2.1. Substrate Preparation

Silicon nanotrees were synthesized in a one-step process by the VLS method inside the low-pressure chemical vapor deposition (LPCVD) reactor. The LPCVD reactor was a quartz tube of 180 cm in length and 14 cm in diameter. Prior to VLS synthesis, silicon test grade wafers (p-type, (0–10) Ω cm, with <100> orientation) were cleaned in an ultrasound bath, first in acetone and then in ethanol at 40 °C for 20 min. The following step includes the standard RCA (Radio Corporation of America) cleaning processes [31]. Cleaned wafers were metal plated by sputtering in Polaron E5000 coater with ~2 nm thick layers of Ag and Au.

2.2. Characterization Techniques

The morphology of the synthesized samples was monitored with a Jeol JSM 7000 F scanning electron microscope under 10 kV discharge and a HitachiS4300-CFE instrument with 5 kV acceleration voltage. Raman spectroscopy measurements on Ag-plated samples were performed utilizing a Jobin Yvon T64000 Raman spectrometer with 532 nm laser wavelength. The microscope objective of 50 \times magnification, 0.75 numerical aperture and 532 nm pump power of 1–2 mW on the sample were used. The signal accumulation time during the Raman measurement was 10 s per scan. Several spectra were obtained in different sample points and averaged. Au-plated samples were measured by a Renishaw 1000B Raman spectrometer utilizing 633 nm laser, 50 \times (0.5 numerical aperture) objective, 5 accumulations and 30 s acquisition time. SERS substrates' quality was tested utilizing Mercaptophenylboronic acid (MPBA) with concentrations of 10^{-4} , 10^{-5} and 10^{-6} M in ethanol. Prepared samples were immersed in MPBA solution and left overnight.

2.3. Silicon Nanotree Synthesis

(a) High-density trunk nanostructure growth

High-density trunk nanostructure growth is obtained by Ag-Au plating before VLS. This topic is already described in our previous work [21] in more detail. In short, wafer plating with Ag before Au increases the number of metal droplets more than 2 times which consequently gives a higher number of SiNWs, i.e., trunks for SiNTrs. In this work, we utilized 300 sccm of 15% forming gas for annealing at 500 °C for one hour. The growth of SiNW trunks is performed at various temperatures from 520–555 °C, while deposition time was 17 or 20 min. In all experiments, 26% SiH₄ diluted in Ar with 420 sccm flow and a partial pressure of 0.07 mbar was utilized.

(b) Branch synthesis

Branches' growth was activated by a simultaneous temperature and gas pressure drop as shown in Figure 1. In this work, we showed two different approaches for branches' growth named (a) 'shots', and (b) 'cycles'. The first approach includes a variation of SiH₄ gas shots number (Figure 1a). This approach was tested for different initial temperatures, i.e., the trunk growth temperatures were 555, 545, 535, and 520 °C. The second, the 'cycles' approach, is based on repeating the heating–cooling cycles with only one gas shot per cycle (Figure 1b). After the trunk synthesis, it is necessary to trigger the catalyst droplet diffusion along their facets. For that reason, the LPCVD tube was vacuumed to the minimum value, in our case to 0.001 mbar, and as the pressure minimum is reached, the heating was turned off. After the temperature decreased for 10 °C (shots approach) or 5 °C (cycles approach), the SiH₄ gas shot of 0.25 mbar was introduced. Hence, we used a simultaneous decrease of temperature and SiH₄ pressure within the reaction chamber for branches' growth. The temperature decrease rate was (3.4 ± 0.1) °C/min in all cases. For example, in Figure 1a, the trunks were grown at 555 °C for 17 min. After closing all gasses, the system was vacuumed

and the heating was switched off. Once the temperature dropped to 545 °C the first gas shot was introduced for 30 s followed by a pause for 60 s while only the temperature was decreasing. The number of shots varied from 1 to 4. In Figure 1b, the trunks' growth was at 520 °C while only one gas shot was introduced for 4–5 min. starting at 515 °C. Afterwards, the temperature was increased to 520 °C and the whole process was repeated 1–4 times. Forming gas with the partial pressure of 0.2 mbar was included in each fabrication step apart from the SiH₄ shots periods.

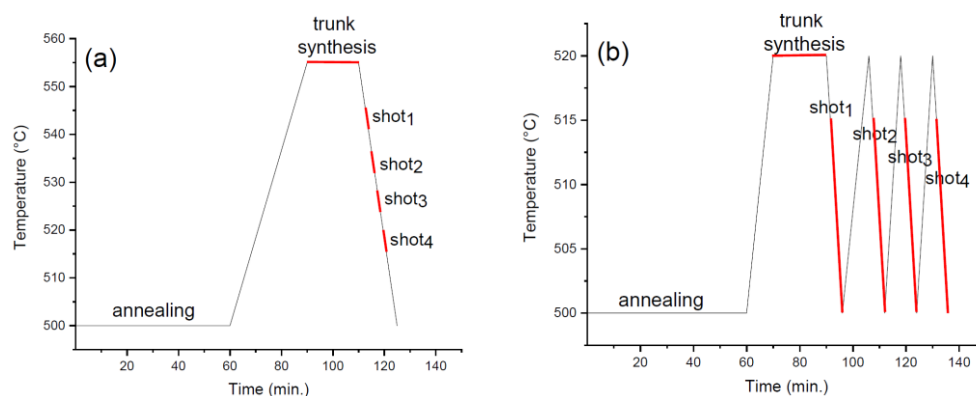


Figure 1. Scheme of silicon nanotrees synthesis steps synthesized by low-pressure chemical vapor deposition: (a) Four Silane shots in one temperature drop, (b) Four cycles with one Silane shot per cycle.

3. Results

3.1. Morphology of SiNTR

3.1.1. Synthesis Method A—Temperature Dependence on SiNTr Growth

Utilizing the synthesis method–(a)–, we selected two shots as the fixed-parameter while the trunk synthesis temperature was 555 °C, 545 °C, 535 °C and 520 °C. The trunks' synthesis temperatures are correlated with the branches' growth temperatures in a way that the first shot started 10 °C below the trunks' synthesis temperature. As shown in Figure 2, the branch' density decreases with the temperature if, for example, Figure 2a,d are compared. The difference in branch density for the growth at 545 °C and 535 °C (Figure 2b,c) cannot be estimated straightforwardly. The trunks' and branches' thicknesses increase with the temperature increase (Figure S1) as expected.

Figure 3 shows samples synthesized at 535 °C with an increasing number of SiH₄ shots during the cooling process. What is observed is a significant increase in branches' density especially when 1–2 and 3–4 shots are compared. To support this result, the analog SEM figures for trunk growth at 545 °C are provided in Figure S2.

3.1.2. Synthesis Method B—Branch Density in Correlation with Cycle Numbers

Figure 4 shows samples fabricated by a single Silane shot per cycle. SEM figures with lower magnification are shown in Figure S3. The trunks' synthesis temperature was 520 °C for 20 min., while the gas injection temperature was 515 °C. As the cycle number increased, the density of the branches increased as well. The cross-section showed that the NTr height was around 2.5 μm, while the trunks' thickness increased from (67 ± 16) nm to (110 ± 10) nm (Figure S4). With the cycle number increase, the branches' thickness increased from (17 ± 3) nm (Figure S4a) to (28 ± 5) nm (Figure S4b).

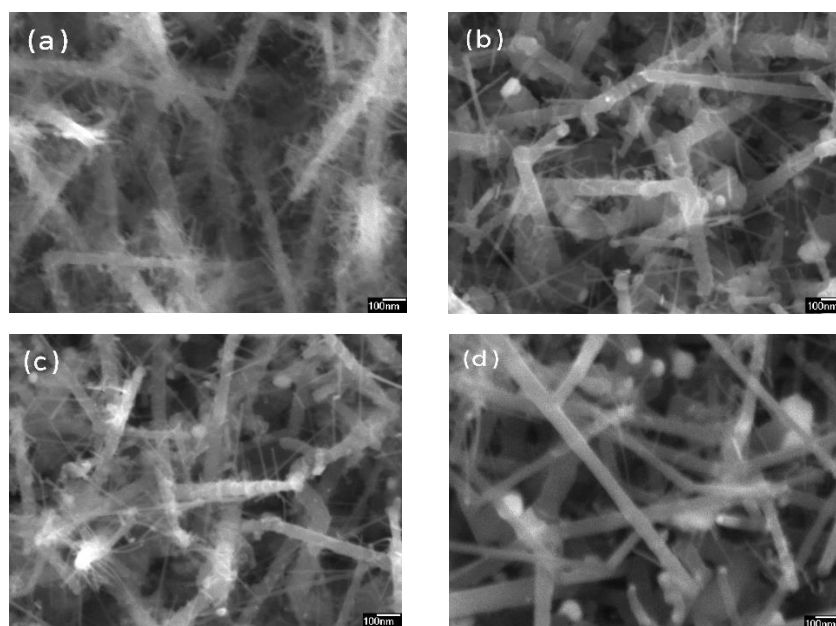


Figure 2. SiNTr synthesized by two Silane shots. The trunks' growth temperature was (a) 555 °C, (b) 545 °C, (c) 535 °C and (d) 520 °C.

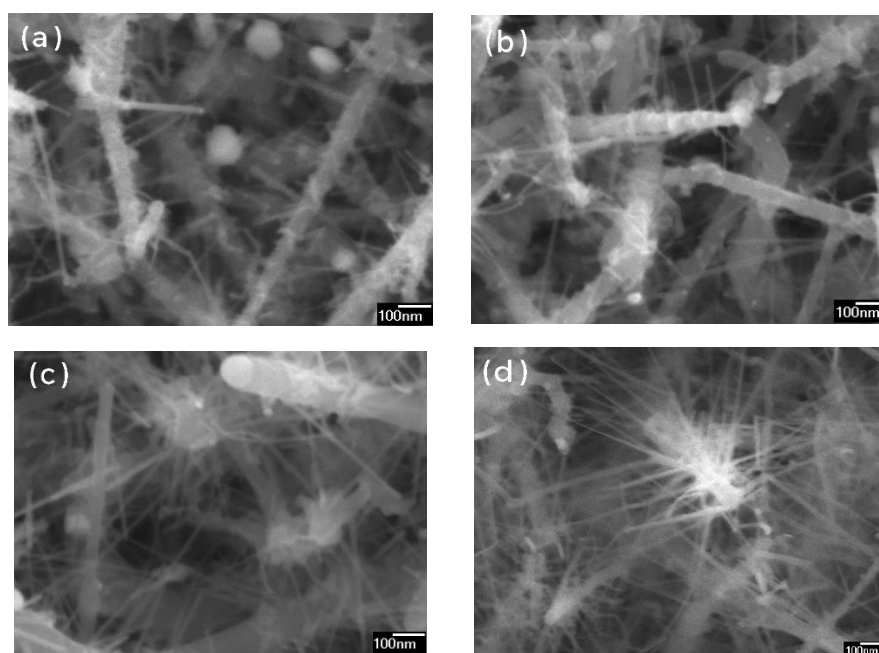


Figure 3. Samples were synthesized at 535 °C with different Silane shots number: (a) one shot, (b) two shots, (c) three shots, and (d) four shots.

3.2. The Flexibility of the Structure in Correlation with Metal Plating

In this section, it is shown that the substrate nanostructure is sensitive to liquid immersion depending on the metal coating layer. Figure 5a shows a dry NTr substrate coated with a ~10 nm Ag layer, while Figure 5b is the same nanostructure but after immersion in water. Figure 5c shows the same pristine nanostructure as in Figure 5a, however, coated with a ~40 nm Ag layer and it is correlated with Figure 5d obtained after immersion in water. It is observed that branches change their position in the case of thin layer coating (Figure 5b), while preserving the same position for a thicker layer (Figure 5d). To additionally support these results, see Figures S6 and S7. The flexibility of the nanostructure was monitored for

8, 10, 14, 20, 30, and 40 nm Ag layer thicknesses (Figure S7). SEM figures have shown that for coatings 8–20 nm there is a strong change in nanostructure after wetting, while it is not the case for samples with coating layers from 30 to 40 nm.

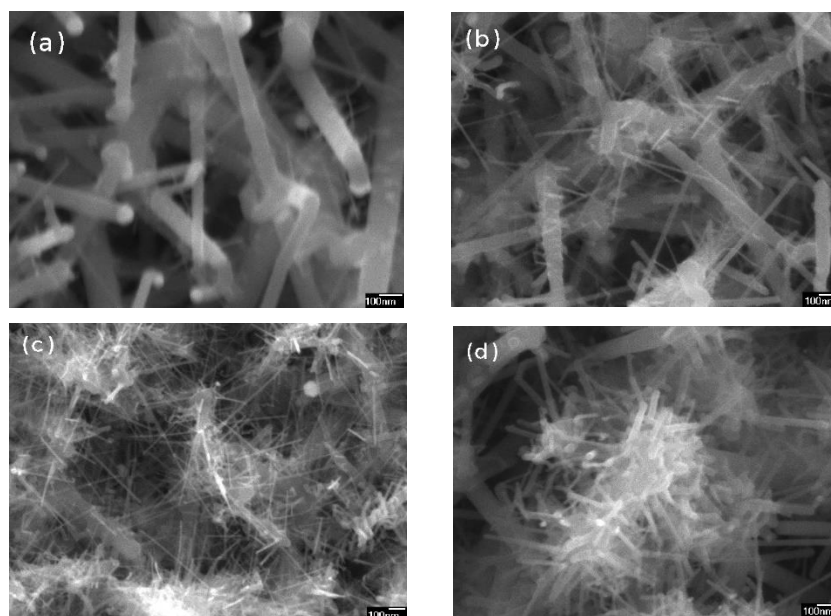


Figure 4. Branch density in correlation with cycle number: (a) one cycle, (b) two cycles, (c) three cycles and (d) four cycles.

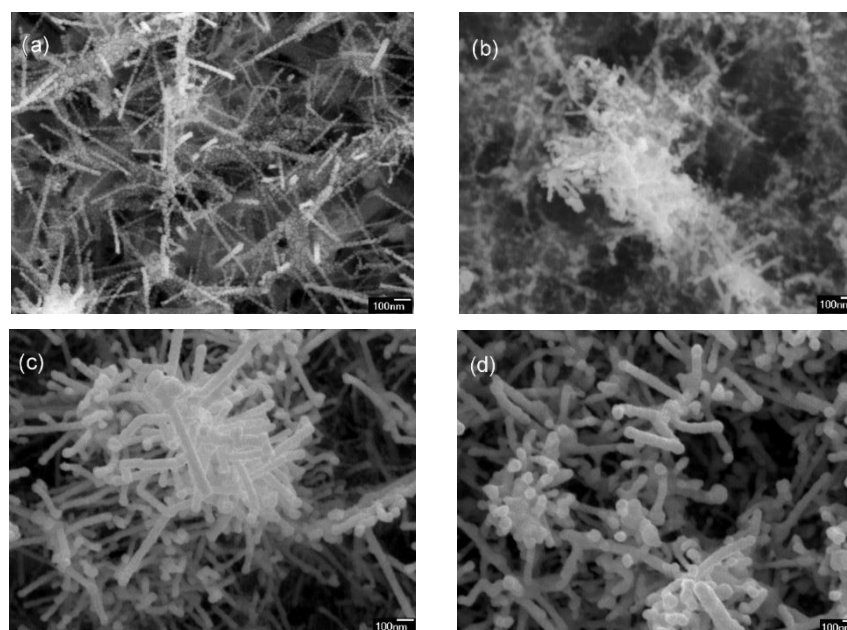


Figure 5. NTr nanostructure changes after immersion in water depending on Ag coating layer thickness: (a) 10 nm Ag layer dry [32], (b) 10 nm Ag layer after wetting, (c) 40 nm Ag layer dry and (d) 40 nm Ag layer after wetting.

3.3. SERS

Figure 6 shows an example of SERS spectra for two different laser excitations, 532 and 633 nm. In both cases, SiNTr nanostructure was obtained by changing the shots number. The extracted values of the intensity at 1073 cm^{-1} are shown in Figures 7 and 8. Figure 7 shows the SERS intensities of 10^{-5} M MPBA at 1073 cm^{-1} monitored by 532 nm laser. An example of the spectra is shown in Figure S8, and MPBA bands are explained in our

previous work [20]. Temperature dependence (red line) on SERS features corresponds to samples shown in Figure 2. The results showed maximum SERS intensities for trunk synthesis between 535–555 °C. Samples synthesis at 535 °C with the increasing number of shots in one cycle, corresponding to Figure 3, have shown an optimum range of 2–4 shots (solid blue line). In the case of changing the number of cycles (which corresponds to samples in Figure 4 labeled with a dotted blue line), the maximum SERS intensity was obtained for two cycles. All samples were coated with a 10 nm Ag layer and therefore subject to nanostructure change after immersion in MPBA.

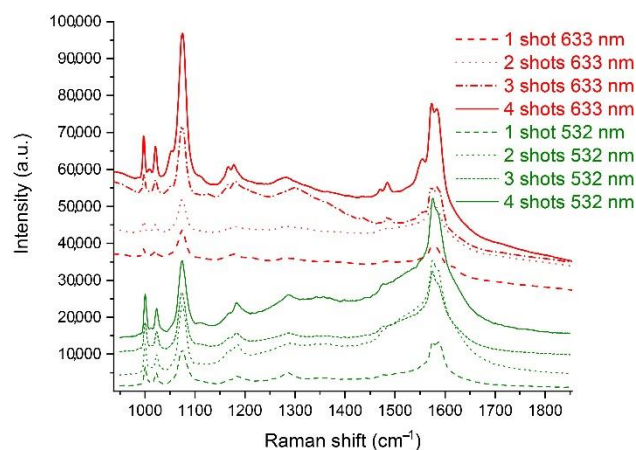


Figure 6. MPBA spectra for 633 and 532 nm laser excitations.

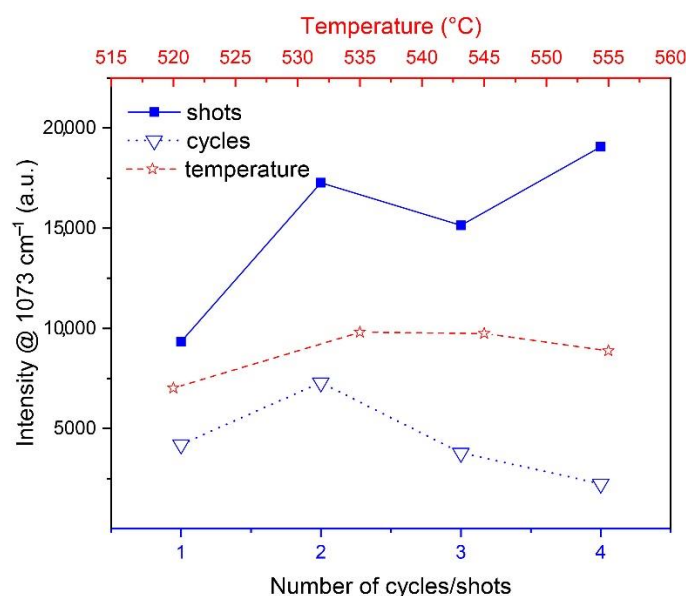


Figure 7. SERS intensity values of MPBA band at 1073 cm^{-1} for various cycles, shot numbers and temperatures.

Figure 8 shows the SERS intensities of 10^{-4} , 10^{-5} and 10^{-6} M MPBA at 1073 cm^{-1} monitored by 633 nm laser. The samples synthesized at 545 °C were plated with Au (Figure S9). The analytical enhancement factor (AEF) was calculated as described in [33,34], and labeled with the red-dot line for each corresponding concentration (Figure 8). To confirm a good homogeneity and repeatability of the SERS signal on this type of substrate, mapping of one sample was performed (Figure S10 and additional example Figure S11) and obtained the relative standard deviation (RSD) 5.3% at 1073 cm^{-1} .

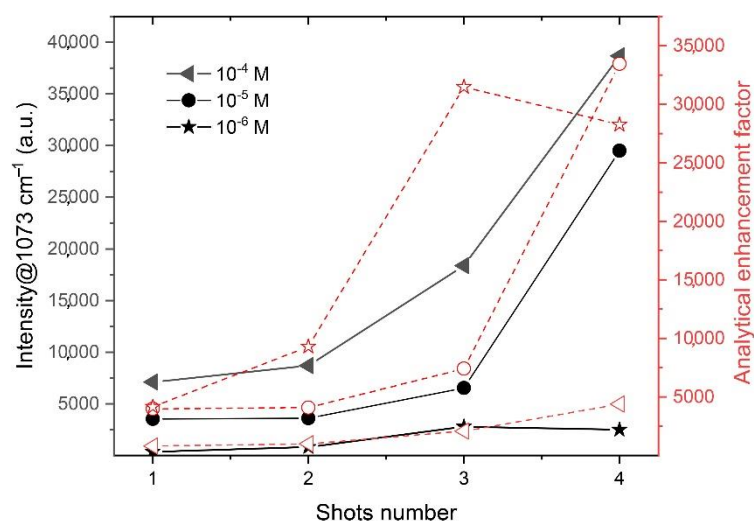


Figure 8. SERS intensity at 1073 cm^{-1} obtained by 633 nm laser excitation and calculated analytical enhancement factor for different MPBA concentrations.

4. Discussion

4.1. Discussion on NTr Nanostructure and SERS

In our previous works [20,21], we discussed the optimization of silicon nanowires which play the role of nanotrees' trunks in this work. One of the beneficial parameters for high SERS enhancement is high trunk density and elasticity. In this work, we used achievements from the previous research [21], i.e., the silicon wafers were plated with Ag-Au to increase the number of trunks per unit area by over two times and reduce their thickness.

The following nanostructure optimization parameter is the synthesis temperature. In our previous work [20] it is shown that the optimal synthesis temperature of silicon nanowires for SERS applications is $500\text{ }^{\circ}\text{C}$. However, this temperature was not adequate for branches' growth. Since the branches' growth requires a temperature drop, the trunk synthesis at $500\text{ }^{\circ}\text{C}$ would lead to the branches' synthesis under $500\text{ }^{\circ}\text{C}$ which in our experiments did not provide adequate branch growth. Therefore, the first goal was to find the optimal synthesis temperature. In order to explore the branches' growth, we selected 'two shots' as the fixed parameter, and changed the synthesis temperature. Figure 2 shows the increase in branch length and thickness as the temperature increases, which is in agreement with wire growth dynamics described in [21]. Typical branch thickness ranges from $9\text{--}15\text{ nm}$ and trunks' from $50\text{--}60\text{ nm}$.

Furthermore, we selected $535\text{ }^{\circ}\text{C}$ as the fixed parameter and changed the number of shots during a single cycle. SEM, as seen in Figure 3, showed an increase in branch length and thickness as the number of shots increased. Since it is challenging to calculate the branches' length distribution and density, we can only estimate that these parameters are significantly higher for three and four shots than for one and two. The fourth shot gives a slight contribution to branches' growth since it is performed at lower temperatures, which causes a low growth rate. The minimum and maximal measured branch thicknesses were 7 nm and 20 nm , respectively.

To preserve the elasticity of trunks and the 'tweezers effect' [20], the idea was to synthesize trunks at as low of a temperature as possible. A detailed explanation of axial trunk growth rate in its dependence on temperature, partial gas pressure and deposition time is given in [21]. The lowest trunk synthesis temperature at which we could obtain branches was $520\text{ }^{\circ}\text{C}$, i.e., the branches were synthesized between $515\text{--}500\text{ }^{\circ}\text{C}$. Since we wanted to increase the number of branches and their thickness the cycle was repeated up to four times as described in the second synthesis approach. SEM images in Figure 4. shows very weak branch density after one shot and high branch density after four cycles. Obtained trunk thickness was ranging from $66\text{ to }110\text{ nm}$ while branches ranged from $11\text{ to }110\text{ nm}$.

28 nm. Although trunk thickness is low after one cycle, it increases with the number of cycles and the main idea of preserving the trunks' thickness was not completely successful. However, this is an adequate way for NTr fabrication, since one can control the trunks' and branches' growth by increasing or decreasing the number of cycles.

SERS measurements (Figure 7) show the highest intensity for NTrs whose trunks have grown between 535–555 °C and utilize 2–4 shots in a single temperature drop (the first synthesis approach). In the case of the second synthesis approach, the SERS intensity of the substrate with two cycles was the highest. It is important to underline that the shot duration in the cycle approach was 4–5 min, i.e., significantly longer than when the synthesis temperature was higher than 520 °C. Short shots such as 30 s at low temperatures (500–515 °C) would not enable adequate branch growth. For the highest SERS performances, it is recommended to synthesize a large number of branches in order to increase the number of hot-spots. However, the best SERS performances and corresponding maximum branch density will be limited by the lacunarity and fractal dimension parameters.

Further confirmation of the branches' influence on SERS intensity and enhancement factor can be seen in Figure 8. The laser excitation at 633 nm shows the optimal region for the samples obtained with three and four shots. These results are in the agreement with the measurements with 532 nm excitation, where the sample with four shots showed the best intensity values. The branches' impacts are more obvious at 10^{-4} and 10^{-5} M than at 10^{-6} M MPBA concentrations.

The highest AEF demonstrated on the Au-plated SiNTR sample was 3.5×10^4 which puts them in a category of good, but not excellent, substrates. The literature [35–37] reports on hierarchical structures with advanced enhancement factors. In all examples, the large surface area of Si-ZnO nanoflower [35], Ag-nanotrees [36], and, Ag-nanostars on Au-nanowires [37] was an important factor. In the present work, the fabrication process was examined over a wide range, and the nanostructure has a large specific surface area, further progress could be looked for in metal plating optimization.

4.2. Additional Optimization Parameters

Previous works show the advantage of a flexible nanostructure for SERS applications [20,28]. A flexible and random-oriented silicon wires nanostructure is reported as the advanced structure for SERS applications due to the 'tweezers effect' and enhanced SERS amplification. Randomly oriented nanowires are shown as a better candidate for SERS substrates in comparison with aligned ones due to the larger number of crossings [38]. One of the main tasks of this paper is to explore the influence of flexible branches on SERS enhancement. Dry and randomly oriented silicon NTrs are schematically shown in Figure 9a. After wetting, trunks lean towards each other and metal-plated branches bend towards the related trunk, creating additional hot spots by the 'tweezers effect' (Figure 9b). In this paper, we demonstrated that branches with 10–20 nm thickness and an 8–20 nm Ag plating layer are adequate to perform the 'tweezers effect', i.e., the silicon NTr nanostructure is flexible after water immersion (Figure 5 and Figure S7). g plating layers thicker than 20 nm fix the nanostructure, and no additional nanowire bending is possible. For that reason, in this paper, we fabricated a 10 nm plating layer which is not the real layer, but the droplets' thickness, since SiNTr facets were plated in an island-like pattern (Figure S12). To prove the flexibility contribution, we performed another experiment utilizing red laser excitation in the following way. One SERS substrate was immersed into 10^{-5} M MPBA, while the second substrate was first immersed in mQ water, dried, and then immersed in MPBA. As we can see, the intensity drops in the case when the substrate was immersed in water and dried to about 40% at 1073 cm^{-1} (Figure S13).

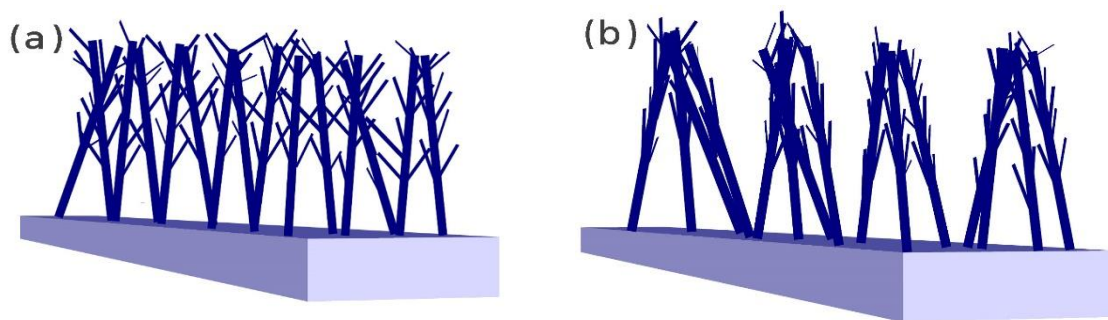


Figure 9. Scheme of randomly oriented silicon NTrs: (a) dry, (b) after wetting.

Apart from metal plating, another parameter that influences SERS performances is fractal dimension and lacunarity. Our experimental observation shows that it is not satisfactory to increase only the fractal dimension, i.e., branches' density. Samples with high trunk and branch density appeared almost black due to the trapping of visible light. However, their SERS performances were not advanced. A similar observation was reported by Yang et al. [39]. Although the highly fractal nanostructure enables multiple light reflections, and intense light–metal and light–molecule interactions, the light trapping prevents the collection of the SERS signals. Our previous paper [18] showed that apart from the fractal dimension, lacunarity should be taken into account as well. Here, we focused on the synthesis approaches and preliminary results so the exact values of fractal dimension and lacunarity are the subject of further research.

4.3. Issues and Limitations

Both synthesis approaches have some issues and limitations. The most important is the branches' regrowth. When the gas shots are applied, branches grow not only from the metal droplets on the trunks' facets, but also from the metal seed on top of the trunk. That creates an additional nanowires layer which does not have as a high density as the primary growth layer (Figure S12), and consequently a drop in SERS intensity occurs. This issue is particularly challenging to avoid since each shot or cycle increases the chance for regrowth as well. One possibility to diminish this issue is to adjust the shot duration. We tried three different shot durations for the trunks' growth at 535 °C. The shot deposition was 90 s in total and in each case. For example, the first sample had six shots with 15 s, the second sample had three shots with 30 s, and the third sample had one shot with 90 s of deposition. SEM in Figure S15 shows weaker branch growth in the case of 15 s shots, while 30 s and 90 s showed a similar structure. The MPBA SERS intensity at 1073 cm^{-1} shows better performances of the sample with 30 s shots (Figure S16). Shots of 15 s are too short, since the gas was pumped out quickly and the branches' growth rate was low. The short duration of 30 s has an advantage over 90 s, i.e., it is easier to design desirable NTr density, length and thickness with several shorter shots than with one long. Therefore, for optimal SERS features and to diminish regrowth, a minimum number of short shots is required.

The idea behind performing several shots and varying their length was to obtain hyper-branched architecture. However, it was not occurring. The branches' thicknesses of 10–20 nm were too thin to allow the growth of even thinner branches on their facets. Similarly, we speculate that it would be challenging to synthesize 10–20 nm thick branches on trunks under 40 nm in diameter. In our experiments, trunk thicknesses were in the range of 50 nm to 110 nm depending on synthesis temperature and shots/cycles number. Therefore, we assume to be close to the experimental edge, considering the features of our laboratory equipment.

5. Conclusions

This paper showed how to synthesize silicon nanotrees using low-pressure chemical vapor deposition utilizing SiH_4 . The nanotree structures were tested for SERS applications

on MPBA molecules. The sensors' properties were determined by the substrate morphology, which include branch thickness, length, density, and metal plating. Two different synthesis approaches were demonstrated based on changing shots or cycles number. By these methods, it is possible to change branch density, length and thickness. To obtain an SERS substrate based on silicon nanotrees, the following parameters should be considered:

- Branches can be successfully synthesized during simultaneous temperature and gas pressure decrease
- The high number of trunks per unit area can be achieved using Ag-Au catalysts
- Forming gas improves branch synthesis
- The synthesis temperature for branch growth should be above 500 °C, while 0.25 mbar SiH₄ shots are used
- Metal plating should be below 20 nm to preserve branch elasticity
- Trunk regrowth can be diminished by minimizing shot/cycle duration and number
- Branches contribute to SERS, however, there is a certain density that should not be traversed

This work determines the synthesis parameters for optimization of the SERS substrates based on nanotree structure. Further optimization should be carried out for the following parameters: trunk height, fractal and lacunarity ratio, SERS optimization at low test-molecules concentrations.

Supplementary Materials: The following supporting information can be downloaded at: <https://www.mdpi.com/article/10.3390/chemosensors10120534/s1>, Figure S1: Trunks' and branches' thicknesses for different temperatures growth.; Figure S2: Si trunks' of the SERS substrate synthesized at 545 °C for 17 min. Branches were obtained by Silane shots: (a) 1 shot, (b) 2 shots, (c) 3 shots, and (d) 4 shots.; Figure S3: SEM figures of samples synthesized at 520 °C utilizing method 'b': (a) 1 cycle, (b) 2 cycles, (c) 3 cycles, (d) 4 cycles.; Figure S4: Cross-section of samples synthesized at 520 °C utilizing method 'b': (a) 1 cycle, (b) 4 cycles.; Figure S5: Branches' thickness for samples synthesized at 520 °C utilizing method 'b': (a) 1 cycle, (b) 4 cycles.; Figure S6: NTrs nanostructure before and after water immersion: (a) pristine SiNTrs nanostructure, (b) dry substrate with 14 nm Ag coating layer, (c) wet dry substrate with 14 nm Ag coating layer.; Figure S7: NTrs nanostructures change for various Ag coating thicknesses before and after water immersion: (a) 8 nm Ag layer, dry substrate, (b) 8 nm Ag layer after wetting, (c) 10 nm Ag layer, dry substrate, (d) 10 nm Ag layer after wetting, (e) 14 nm Ag layer, dry substrate, (f) 14 nm Ag layer after wetting, (g) 20 nm Ag layer, dry substrate, (h) 20 nm Ag layer after wetting, (i) 30 nm Ag layer, dry substrate, (j) 30 nm Ag layer after wetting, (k) 40 nm Ag layer, dry substrate, (l) 40 nm Ag layer after wetting.; Figure S8: SERS spectra of 10 nm Ag coated NTrs substrates for various shots numbers. The substrates were synthesized at 535 °C for 17 min. 20 spectra of each sample were monitored and averaged.; Figure S9: SEM figures of Au plated silicon nanotrees: (a) 1 shot, (b) 2 shots, (c) 3 shots, (d) 4 shots.; Figure S10: Standard deviation after mapping of silicon nanotrees SERS substrate immersed into MPBA concentration of 10⁻⁵ M.; Figure S11: Map of Au-plated nanotrees obtained by '3 shots' and corresponding averaged spectra of 10⁻⁵ M MPBA. Map parameters: step 10 μm, scan sized 50 × 50 μm, the number of points 121.; Figure S12: Example of Ag-plated substrate with island-like structure. The sample's trunks were synthesized at 545 °C for 17 min and 3 shots were performed.; Figure S13: The contribution of a flexible nanostructure for MPBA detection.; Figure S14: SEM, NTr cross-sections examples: (a) regrowth at 545 °C and 5 shots, (b) regrowth at 535 °C and 3 shots, (c) no-regrowth sample, 3 shots at 535 °C, (d) no-regrowth sample, 2 shots at 545 °C.; Figure S15: Shot duration variation: (a) 15 s (6 shots), (b) 30 s (3 shots), (c) 90 s (1 shot). Trunks were synthesized at 535 °C for the same time duration, 17 min.; Figure S16: SERS intensities of 10⁻⁶ M MPBA for samples correlated with Figure S12.

Author Contributions: Conceptualization, H.G.; Methodology, H.G.; Software, I.C.; Formal analysis, M.I.; Investigation, H.G. and P.P.; Data curation, H.G., I.C. and V.G.; Writing—review & editing, H.G.; Supervision, M.I. All authors have read and agreed to the published version of the manuscript.

Funding: This research was funded by the Croatian Government and the European Union through the European Regional Development Fund—the Competitiveness and Cohesion Operational Program (grant number: KK.01.1.1.01.0001), the János Bolyai Research Scholarship of the Hungarian Academy of Sciences (grant number: BO/348/20), the New National Excellence Program of the Ministry of

Human Capacities (grant number: ÚNKP-22-5-DE-407) and the New National Excellence Program of the Ministry of Human Capacities (grant number: ÚNKP-22-3-II-DE-53).

Institutional Review Board Statement: Not applicable.

Informed Consent Statement: Not applicable.

Data Availability Statement: Not applicable.

Conflicts of Interest: The authors declare no conflict of interest.

References

1. Wagner, R.S.; Ooherty, C.J. Mechanism of Branching and Kinking during VLS Crystal Growth. *J. Electrochem. Soc.* **1968**, *115*, 93. [[CrossRef](#)]
2. Cheng, C.; Fan, H.J. Branched nanowires: Synthesis and energy applications. *Nano Today* **2012**, *7*, 327–343. [[CrossRef](#)]
3. Thissandier, F.; Gentile, P.; Brousse, T.; Bidan, G.; Sadki, S. Are tomorrow's micro-supercapacitors hidden in a forest of silicon nanotrees? *J. Power Sources* **2014**, *269*, 740–746. [[CrossRef](#)]
4. Xu, Q.; Meng, G.; Han, F. Porous AAO template-assisted rational synthesis of large-scale 1D hybrid and hierarchically branched nanoarchitectures. *Prog. Mater. Sci.* **2018**, *95*, 243–285. [[CrossRef](#)]
5. Zhang, Y.; Liu, H. Nanowires for high-efficiency, low-cost solar photovoltaics. *Crystals* **2019**, *9*, 87. [[CrossRef](#)]
6. Dhalluin, F.; Desf, P.J.; den Hertog, M.L.; Rouvire, J.L.; Ferret, P.; Gentile, P.; Baron, T. Critical condition for growth of silicon nanowires. *J. Appl. Phys.* **2007**, *102*, 094906. [[CrossRef](#)]
7. Wan, Q.; Huang, J.; Xie, Z.; Wang, T.; Dattoli, E.N.; Lu, W. Branched SnO₂ nanowires on metallic nanowire backbones for ethanol sensors application. *Appl. Phys. Lett.* **2008**, *92*, 102101. [[CrossRef](#)]
8. Zhou, W.; Dai, X.; Lieber, C.M. Advances in nanowire bioelectronics. *Rep. Prog. Phys.* **2017**, *80*, 16701. [[CrossRef](#)]
9. Jung, Y.; Ko, D.K.; Agarwal, R. Synthesis and structural characterization of single-crystalline branched nanowire heterostructures. *Nano Lett.* **2007**, *7*, 264–268. [[CrossRef](#)]
10. Dick, K.A.; Deppert, K.; Larsson, M.W.; Mårtensson, T.; Seifert, W.; Wallenberg, L.R.; Samuelson, L. Synthesis of branched “nanotrees” by controlled seeding of multiple branching events. *Nat. Mater.* **2004**, *3*, 380–384. [[CrossRef](#)]
11. Bierman, M.J.; Jin, S. Potential applications of hierarchical branching nanowires in solar energy conversion. *Energy Environ. Sci.* **2009**, *2*, 1050–1059. [[CrossRef](#)]
12. Song, M.; Zhang, Y.; Chun, J.; Hu, S.; Tang, M.; Li, D. Effects of catalyst droplets on wire growth and the resulting branched structures during VLS growth. *Nanoscale* **2020**, *12*, 7538–7543. [[CrossRef](#)]
13. Yan, C.; Li, X.; Zhou, K.; Pan, A.; Werner, P.; Mensah, S.L.; Vogel, A.T.; Schmidt, V. Heteroepitaxial growth of GaSb nanotrees with an ultra-low reflectivity in a broad spectral range. *Nano Lett.* **2012**, *12*, 1799–1805. [[CrossRef](#)]
14. Cheng, C.; Liu, B.; Yang, H.; Zhou, W.; Sun, L.; Chen, R.; Yu, S.F.; Zhang, J.; Gong, H.; Sun, H.; et al. Hierarchical assembly of ZnO nanostructures on SnO₂ backbone nanowires: Low-temperature hydrothermal preparation and optical properties. *ACS Nano* **2009**, *3*, 3069–3076. [[CrossRef](#)]
15. Zhang, C.; Tian, W.; Xu, Z.; Wang, X.; Liu, J.; Li, S.L.; Tang, D.M.; Liu, D.; Liao, M.; Bando, Y.; et al. Photosensing performance of branched CdS/ZnO heterostructures as revealed by in situ TEM and photodetector tests. *Nanoscale* **2014**, *6*, 8084–8090. [[CrossRef](#)]
16. Dong, A.; Tang, R.; Buhro, W.E. Solution-based growth and structural characterization of homo- and heterobranched semiconductor nanowires. *J. Am. Chem. Soc.* **2007**, *129*, 12254–12262. [[CrossRef](#)]
17. Gebavi, H.; Ristić, D.; Baran, N.; Mikac, L.; Mohaček-Grošev, V.; Gotić, M.; Šikić, M.; Ivanda, M. Horizontal silicon nanowires for surface-enhanced Raman spectroscopy. *Mater. Res. Express.* **2018**, *5*, 015015. [[CrossRef](#)]
18. Risović, D.; Gebavi, H.; Ivanda, M. Influence of fractal and lacunar characteristic of a nanostructured substrate on SERS enhancement. *Appl. Surf. Sci.* **2021**, *537*, 147915. [[CrossRef](#)]
19. Bousiakou, L.G.; Gebavi, H.; Mikac, L.; Karapetis, S.; Ivanda, M. Surface enhanced Raman spectroscopy for molecular identification- A review on surface plasmon resonance (SPR) and localised surface plasmon resonance (LSPR) in optical nanobiosensing. *Croat. Chem. Acta* **2019**, *92*, 479–494. [[CrossRef](#)]
20. Gebavi, H.; Gašparić, V.; Risović, D.; Baran, N.; Albrycht, P.H.; Ivanda, M. Features and advantages of flexible silicon nanowires for SERS applications. *Beilstein J. Nanotechnol.* **2019**, *10*, 725–734. [[CrossRef](#)]
21. Gebavi, H.; Ristić, D.; Baran, N.; Marciuš, M.; Gašparić, V.; Syed, K.; Ivanda, M. Development of silicon nanowires based on Ag-Au metal alloy seed system for sensing technologies. *Sens. Actuators A Phys.* **2021**, *331*, 112931. [[CrossRef](#)]
22. den Hertog, M.L.; Rouvire, J.L.; Dhalluin, F.; Desré, P.J.; Gentile, P.; Ferret, P.; Oehler, F.; Baron, T. Control of gold surface diffusion on Si nanowires. *Nano Lett.* **2008**, *8*, 1544–1550. [[CrossRef](#)] [[PubMed](#)]
23. Doerk, G.S.; Ferralis, N.; Carraro, C.; Maboudian, R. Growth of branching Si nanowires seeded by Au-Si surface migration. *J. Mater. Chem.* **2008**, *18*, 5376–5381. [[CrossRef](#)]
24. Sadeghipari, M.; Mehrvar, L.; Hajmirzaheydarali, M.; Salehi, F.; Mohajerzadeh, S.; Tavassoli, H. Pressure-induced formation of highly controlled branched silicon nanowires suitable for broadband absorption. *J. Mater. Sci. Mater. Electron.* **2016**, *27*, 12903–12912. [[CrossRef](#)]

25. Wang, D.; Qian, F.; Yang, C.; Zhong, Z.; Lieber, C.M. Rational growth of branched and hyperbranched nanowire structures. *Nano Lett.* **2004**, *4*, 871–874. [[CrossRef](#)]
26. Gentile, P.; David, T.; Dhalluin, F.; Buttard, D.; Pauc, N.; den Hertog, M.; Ferret, P.; Baron, T. The growth of small diameter silicon nanowires to nanotrees. *Nanotechnology* **2008**, *19*, 125608. [[CrossRef](#)]
27. Nebolsin, V.A. Critical parameters of quasi-one-dimensional growth of nanowires according to the scheme vapor → liquid drop → crystal. *Mater. Res. Soc. Symp. Proc.* **2011**, *1350*, 24–29. [[CrossRef](#)]
28. Schmidt, M.S.; Hübner, J.; Boisen, A. Large area fabrication of leaning silicon nanopillars for Surface Enhanced Raman Spectroscopy. *Adv. Mater.* **2012**, *24*, OP11–OP18. [[CrossRef](#)]
29. Doerk, G.S.; Radmilovic, V.; Maboudian, R. Branching induced faceting of Si nanotrees. *Appl. Phys. Lett.* **2010**, *96*, 2012–2015. [[CrossRef](#)]
30. Gaboriau, D.; Aradilla, D.; Brachet, M.; le Bideau, J.; Brousse, T.; Bidan, G.; Gentile, P.; Sadki, S. Silicon nanowires and nanotrees: Elaboration and optimization of new 3D architectures for high performance on-chip supercapacitors. *RSC Adv.* **2016**, *6*, 81017–81027. [[CrossRef](#)]
31. Kern, W. The Evolution of Silicon Wafer Cleaning Technology. *J. Electrochem. Soc.* **1990**, *137*, 1887. [[CrossRef](#)]
32. Liu, M.; Sun, L.; Cheng, C.; Hu, H.; Shen, Z.; Fan, H.J. Nanoscale Highly effective SERS substrates based on an atomic-layer-deposition-tailored nanorod array scaffold. *Nanoscale* **2011**, *3*, 3627–3630. [[CrossRef](#)]
33. Pal, P.; Bonyár, A.; Veres, M.; Himics, L.; Balázs, L.; Juhász, L.; Csarnovics, I. A generalized exponential relationship between the surface-enhanced Raman scattering (SERS) efficiency of gold/silver nanoisland arrangements and their non-dimensional interparticle distance/particle diameter ratio. *Sens. Actuators A Phys.* **2020**, *314*, 112225. [[CrossRef](#)]
34. le Ru, E.C.; Etchegoin, P.G. Quantifying SERS enhancements. *MRS Bull.* **2013**, *38*, 631–640. [[CrossRef](#)]
35. Li, S.; Zhang, N.; Zhang, N.; Lin, D.; Hu, X.; Yang, X. Three-dimensional ordered Ag/ZnO/Si hierarchical nanoflower arrays for spatially uniform and ultrasensitive SERS detection. *Sens. Actuators B Chem.* **2020**, *321*, 128519. [[CrossRef](#)]
36. Chen, Y.C.; Hsu, J.H.; Hsu, Y.K. Branched silver nanowires on fluorine-doped tin oxide glass for simultaneous amperometric detection of H₂O₂ and of 4-aminothiophenol by SERS. *Microchim. Acta* **2018**, *185*, 106. [[CrossRef](#)]
37. Zalaffi, M.S.; Litti, L.; Canton, P.; Meneghetti, M.; Moretto, L.M.; Ugo, P. Preparation and characterization of Ag-nanostars@Au-nanowires hierarchical nanostructures for highly sensitive surface enhanced Raman spectroscopy. *Nano Express* **2020**, *1*, 020006. [[CrossRef](#)]
38. Khan, M.A.; Hogan, T.P.; Shanker, B. Gold-coated zinc oxide nanowire-based substrate for surface-enhanced Raman spectroscopy. *J. Raman Spectrosc.* **2009**, *40*, 1539–1545. [[CrossRef](#)]
39. Yang, J.; Li, J.B.; Gong, Q.H.; Teng, J.H.; Hong, M.H. High aspect ratio SiNW arrays with Ag nanoparticles decoration for strong SERS detection. *Nanotechnology* **2014**, *25*, 465707. [[CrossRef](#)]